Shallow lacustrine carbonate microfacies document orbitally paced lake-level history in the Miocene Teruel Basin (North-East Spain)

HEMMO A. ABELS*, HAYFAA ABDUL AZIZt[1], JOSÉ P. CALVOt and ERIK TUENTER§[2]
**Stratigraphy/Paleontology, Dept. of Earth Sciences, Utrecht University, Budapestlaan 4, 3584 CD, Utrecht, The Netherlands (E-mail: abels@geo.uu.nl)*
t*Department of Earth and Environmental Sciences, Geophysics LMU Munich, Theresienstrasse 41, 80333 Munich, Germany*
t*Instituto Geologico y Minero de España (IGME), Ríos Rosas 23, 28003 Madrid, Spain*
§*Royal Netherlands Meteorological Institute (KNMI), P.O. Box 201, 3730 AE, De Bilt, The Netherlands*

ABSTRACT

Results are presented of a detailed carbonate petrographic study of an Upper Miocene lacustrine mixed carbonate–siliciclastic succession in the Teruel Basin (Spain) with the aim of constraining lake-level variability at different stratigraphic scales. Regular alternations of red to green mudstone and lacustrine limestone, termed the 'basic cycle', reflect lake-level variations at the metre-scale. In an earlier study, the basic cycle was shown to be controlled by the climatic precession cycle. Petrographic analysis made it possible to distinguish two main carbonate microfacies groups characteristic of very shallow *transient* and shallow *permanent* lake environments, respectively. In addition to the basic cyclicity, the microfacies analysis reveals lake-level variations on a larger scale. As a consequence, the astronomical forcing hypothesis of the cyclicity in the Cascante section is explored further. A climate modelling study of orbital extremes indicates that high lake levels could relate to enhanced net winter precipitation and runoff during precession minima, consistent with Mediterranean geological data. Using this phase relationship, an astronomical tuning of the cycles is established starting from astronomical ages of magnetic reversal boundaries. Subsequently, successive basic cycles are correlated to precession minima. The tuning reveals an identical number of basic cycles in the Cascante section as precession-related sapropel cycles in the deep marine succession at Monte dei Corvi (Italy), corroborating the precessional control of the basic cycles at Cascante. Lake-level highstands in the large-scale cycle identified by the microfacies analysis relate to maxima in both the *ca* 100 and 405 kyr eccentricity cycles, again consistent with Mediterranean geological data. Subtraction of the identified astronomically related (lake-level) variations from the palaeoenvironmental record at Cascante indicates a shift to deeper and more permanent lacustrine environments in the upper half of the section. The cause of this shift remains unclear, but it may be linked to tectonics, non-astronomical climate, long-period astronomical cycles or autogenic processes.

[1]Present address: Deltares/TNO, Geological Survey of The Netherlands, Princetonlaan 6, 3508 TA, Utrecht, The Netherlands.
[2]Present address: Institute for Marine and Atmospheric Research (IMAU), Utrecht University, Princetonplein 5, 3584 CC, Utrecht, The Netherlands.

Keywords: Astronomical forcing, carbonate petrography, climate modelling continental sediments, cyclostratigraphy, Late Miocene, Spain.

INTRODUCTION

Reconstruction of the evolution of sedimentary environments requires distinction among tectonic, climatic and autogenic processes, which is often difficult to achieve because they may result in similar palaeoenvironmental shifts and act simultaneously as well. However, high-resolution (*ca* 10^4 yr) age control may provide critical information about the forcing mechanisms of the palaeoenvironmental changes. Recent improvements of the Cenozoic, and especially the Neogene, magnetic polarity timescale (Gradstein *et al.*, 2004; Lourens *et al.*, 2004) offer an excellent opportunity to correlate lithological and biological changes in sedimentary successions with well-dated tectonic and (global) climatic events (Dupont-Nivet *et al.*, 2007). The improvements further allow the presence of astronomical climate forcing to be examined, which potentially yields valuable information on the response of palaeoenvironmental and sedimentological processes to known climate variations in terms of relative humidity and seasonality (Weedon, 2003). In addition, the identification and subsequent removal of orbitally induced climate variations from the sedimentary record reveal other variations that may be related to autocyclicity, tectonics or non-astronomical climate-forcing mechanisms.

Neogene continental successions in Spain offer long sedimentary records of low-gradient endorheic basins in which climate and tectonics theoretically have a great impact on the depositional environment (Sanz *et al.*, 1995; Abdul Aziz *et al.*, 2003b). In the present paper, a continued cyclostratigraphic study of the Cascante section in the southern Teruel Basin (NE Spain; Fig. 1) is presented, elaborating on a previous study by Abdul Aziz *et al.* (2004). The section is characterized by a distinct alternation of red to green mudstone, interpreted to be deposited in a distal alluvial floodplain environment, and shallow lacustrine to palustrine limestone (Fig. 2). Magnetostratigraphy and small-mammal biostratigraphy revealed that deposition took place between 9Æ4 and 10Æ2 Ma (Abdul Aziz *et al.*, 2004). Abdul Aziz *et al.* (2004) applied spectral analysis on high-resolution colour records. Results revealed a cyclicity at a 1:2:5 ratio, resembling the ratio of the climatic precession, obliquity and short eccentricity cycles. Combining the statistical and magnetostratigraphic results, those authors showed that the basic, metre-scale mudstone–limestone cycles are related to the precession cycle (Abdul Aziz *et al.*, 2004). However, no palaeoenvironmental significance could be assigned to the other scales of cyclicity that were tentatively attributed to obliquity and short-eccentricity. Consequently, no astronomical tuning of the Cascante section was established. In this study, a detailed sediment petrographic study of all 34 lacustrine and palustrine limestone beds was therefore performed. In addition, simulations with a global climate model were carried out as an independent check on the phase relationship between lake-level highstands and precession as derived from published geological data. Finally, an astronomical tuning of the Cascante succession is presented, allowing a quantification of the influence of climate and tectonic variability on this continental sedimentary environment.

GEOLOGICAL SETTING

In the Teruel Basin (Fig. 1A), a 100 km long and 15 km wide NNE–SSW trending half-graben, sediment deposition started in the Early Miocene and lasted until the Late Pliocene (Anadón & Moissenet, 1996). Sedimentation took place in an internally drained continental setting dominated by red alluvial terrigenous beds, lacustrine and palustrine limestones, and gypsum. The sedimentary succession is characterized by large-scale (40 to 200 m) alternations of red siliciclastic sediments and lacustrine carbonate or evaporitic sediments (Anadón *et al.*, 1997; Alonso Zarza & Calvo, 2000).

The studied Cascante section is located in the southern part of the basin (Fig. 1B), along the Villel-Cascante del Rio road, in the Teruel-Ademuz sub-basin. The sub-basin is flanked by Mesozoic rocks, predominantly composed of Triassic mudstone and evaporite rocks and Jurassic limestone. The presence of gypsum deposits in the basin has been related to leaching of Triassic sediments cropping out along the basin margin (Broekman, 1983; Anadón *et al.*, 1992). The Neogene infill starts at the basin margin with alluvial fan conglomerates and breccias that grade laterally, within a few kilometres, into fine-grained distal alluvial fan sediments and shallow lacustrine deposits towards the centre of the basin.

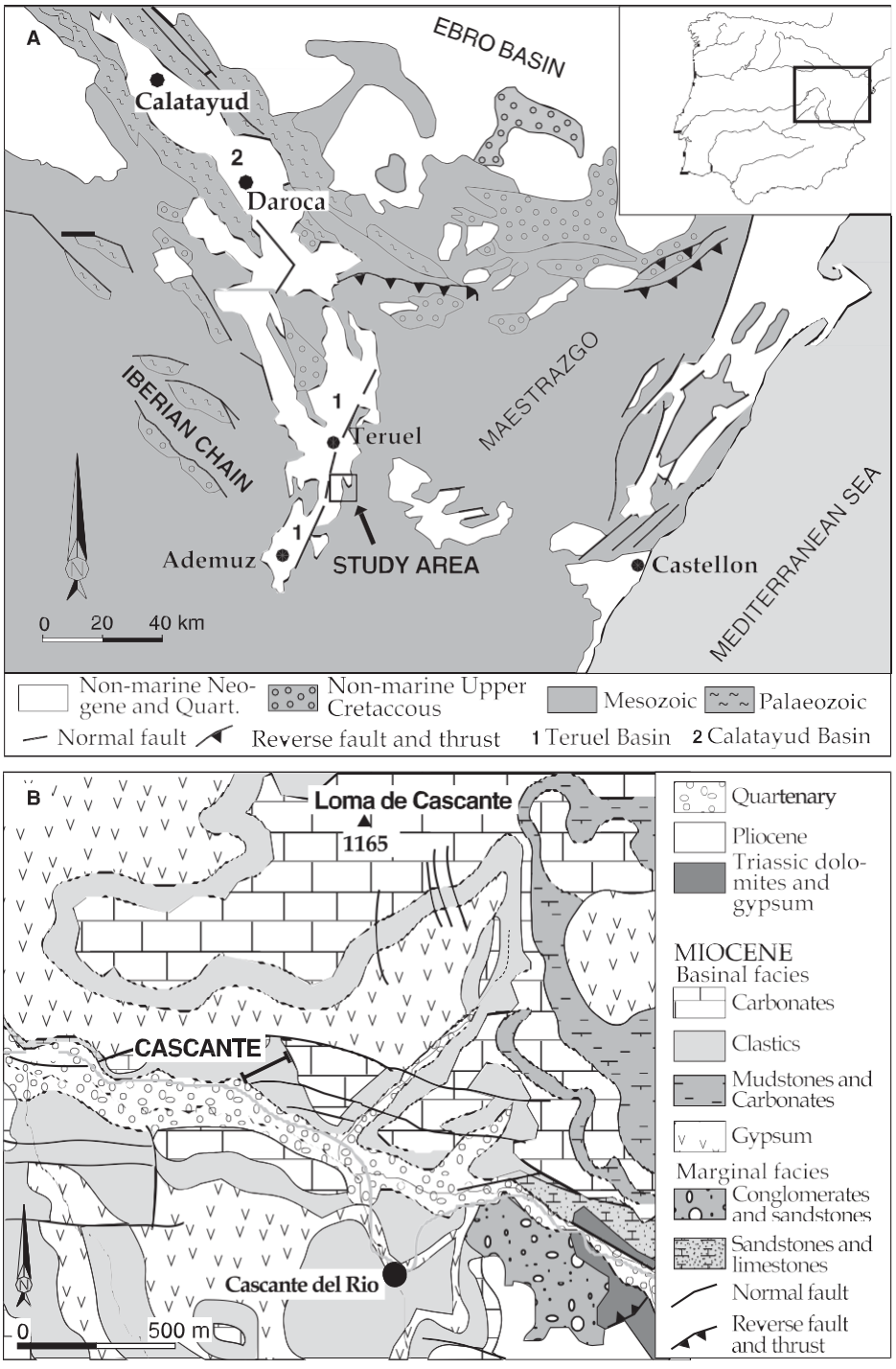

Fig. 1. (A) Geological and location map of the region of the NNE–SSW trending Teruel Basin. (B) Detailed geological map and location map of the Cascante section (after Abdul Aziz, 2001). Miocene basinal facies are depicted in the legend from bottom to top according to their stratigraphic order.

THE CASCANTE SECTION

The studied Upper Miocene section comprises the siliciclastic interval of the Loma de Cascante Formation, one of the formation-scale siliciclastic–limestone alternations in the Teruel Basin (Fig. 2). The lithology is characterized by a distinct regular sedimentary cyclicity of red and green, orange mottled, distal alluvial fan mudstone and white, shallow lacustrine limestone (Abdul Aziz *et al.*, 2004). This basic mudstone–limestone cycle has an average thickness of 2Æ2 m (Abdul Aziz *et al.*, 2004) (Fig. 3). Thirty-four basic cycles were observed in the Cascante

Fig. 2. View to the east of the siliciclastic Cascante section with the limestone unit on top of cycle number 34. Red/green mudstone–white limestone cycles are indicated by numbers in black (except for cycle 25, shown in grey because it is not well visible in the picture). The scale bar is approximately valid for the middle of the photograph (for actual thicknesses, see Fig. 4).

section. A 30 m thick lacustrine limestone unit characterized by metre-scale bedding overlies the mixed carbonate–siliciclastic succession (Fig. 2).

SEDIMENTOLOGY – OUTCROP SCALE

The outcrop data presented in this paper are a compilation of new and published observations and interpretations (Broekman, 1983; Broekman *et al.*, 1983; Kiefer, 1988; Abdul Aziz, 2001; Abdul Aziz *et al.*, 2004). The specific outcrop characteristics of all 34 basic cycles are consistent laterally over a distance of 300 m to the west of the studied section. Some unique mudstone colour patterns in outcrops between 1 and 2 km to the east were proven to be time-equivalent using detailed magnetostratigraphy (Abdul Aziz *et al.*, 2004).

Red and green mudstone

Description

The average thickness of the mudstone part of a basic cycle is 1Æ8 m (ranging from 1Æ4 to 3Æ3 m). The mudstone commonly starts with a dark red colour at the base, gradually changing to orange with upward increasing greyish-green mottling, followed by an often sharp transition to greenish mudstone showing abundant yellow mottling (Fig. 3). The mudstone usually is massive and commonly contains some randomly distributed gypsum aggregates with arbitrarily oriented

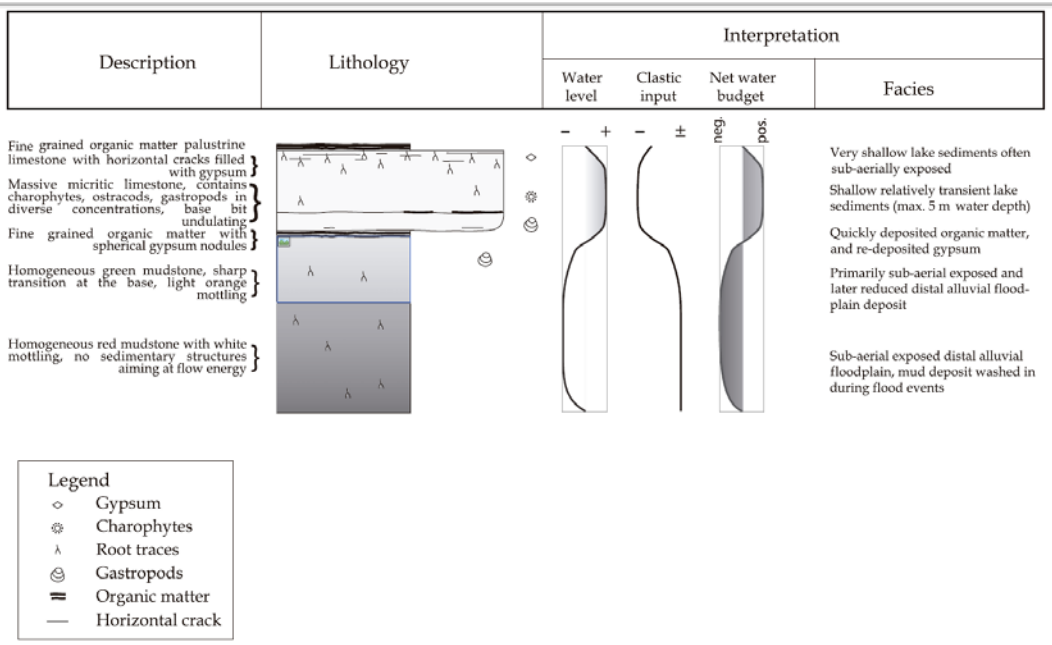

Fig. 3. Basic mudstone–carbonate cycle recognized in the Cascante section with an indication of the main lithofacies features and their sedimentological interpretation.

well-developed crystal structure and few millimetre-grained spherical gypsum nodules. Sparse, millimetre-sized to centimetre-sized carbonate lithoclasts are found locally floating in the mudstone. Illite and smectite are the dominant clay minerals in these mudstones (Abdul Aziz *et al.*, 2004). Freshwater gastropods, bivalves and small-mammal fossil remains are scarce and are specifically concentrated in dark grey, organic-rich centimetre-thick beds (Broekman, 1983; Abdul Aziz *et al.*, 2004). The organic matter is millimetre-grained and originates from plant remains. The organic-rich layers are unconsolidated and occasionally show millimetre-scale lamination. These layers occur beneath, on top of, and locally within the limestone beds; they also contain fragmented charophyte remains and millimetre-scale to centimetre-scale spherical gypsum nodules.

Interpretation

The mudstone deposits are interpreted to have accumulated out of suspension following flood events in distal mudflat areas of alluvial fans on an usually dry and exposed basin floor, in accordance with the interpretation given by Kiefer (1988). Lack of evidence for stream action in the mudstone strata suggests that the supply of mud occurred through flood events that rapidly washed the mud into the basin without causing any apparent erosion. However, the massive internal structure of these deposits only displays indications of root bioturbation by mottling obsuring any sedimentary clues of a transport mechanism. The massive structure could have been caused by extensive mud-cracking and bioturbation because of root activity after deposition. Wright & Marriott (2007) report that these two mechanisms can, together with compaction, easily remove sedimentary structures after deposition. In addition to the removal of all primary sedimentary structures, prolonged sub-aerial exposure caused pervasive oxidation within the mudstone. The green mudstone on top of the red mudstone might be indicative of initially red sediments that were subjected to reduction and leaching after deposition (Eardley *et al.*, 1973; Broekman, 1983; Abdul Aziz *et al.*, 2004). Similar reduction features have also been reported from the Upper Kizilirmak Basin in Turkey (Türkmen & Kerey, 2000) and from the Calatayud Basin in Spain (Abdul Aziz *et al.*, 2003b).

As mentioned above, gypsum is present in the mudstone as aggregates and millimetre-sized spherical nodules, which occur especially in the organic-rich layers just above and below the

limestone beds. The aggregates are interpreted as secondary deposits because of their well-developed crystal structures, random orientation and occurrence. The millimetre-sized spherical nodules, that are found mainly in the organic-rich layers, are interpreted as transported and redeposited gypsum. An alternative origin is interstitial nodular gypsum growth. The absence of (other) clearly primary deposited subaqeous gypsum is remarkable. Warren (1999) reports that deposition of gypsum in continental settings mainly depends on three critical factors: (i) abundant water to evaporate and introduce solutes; (ii) sufficient solutes to precipitate; and (iii) time. Taking into account the ample time for mudstone deposition and the abundance of gypsum sources, i.e. Triassic formations, at the basin margin (Broekman, 1983), the limiting factor for gypsum deposition in the Cascante region is water. Thus, the lack of well-developed gypsum beds could indicate that during mudstone deposition phreatic groundwater levels in the basin were not high enough to reach the solute concentration necessary to precipitate gypsum (Rosen, 1994). This observation suggests that the mudstone deposits accumulated throughout prolonged dry periods during which the basin was flooded only occasionally. The rare small carbonate pebbles are interpreted as relicts of sheet floods that transported larger clasts than average, derived from the Jurassic rocks in the basin margin.

Limestone

Description

The average thickness of limestone beds in the basic cycle is 0Æ5 m (0Æ2 to 0Æ9 m). The limestone beds are poorly laminated or massive, whereas their top parts commonly show vertical tubes and horizontal cracks (Fig. 3). Vertical tubes are a few millimetres in width and usually up to several centimetres in length, but they can reach up to 20 cm in massive limestones. Individual tubes show upward and downward divergent patterns, so that many tubes appear to be interconnected. Millimetre-thick horizontal cracks can be present ubiquitously, especially towards the top of the limestone beds. The cracks and vertical tubes locally produce a fragmented limestone, a feature that is especially visible in the top part of pronounced massive limestones. Fossil remains of complete charophyte stems and gyrogonites, broken and complete gastropods, ostracods and some undifferentiated green algae are found. Rare, very fine sand-sized quartz grains are present. Gypsum is present usually as nodules or as fillings of horizontal cracks and vertical structures (Abdul Aziz, 2001). Fine-grained, organic-rich laminae (see description in the *Red and Green Mudstone* section) are present locally within the limestone beds. The degree of consolidation of the limestone beds depends on the amount of clay, gypsum and organic matter, with high gypsum contents resulting in very consolidated limestones. In the upper part of the section, some limestone beds show undulating structures, with locally centimetre-scale cross-stratification, which are present mainly at the base and in the lower half of the limestone beds.

Interpretation

The limestone beds are interpreted as lacustrine carbonate deposits that accumulated in a shallow lake. The vertical tubes are interpreted as root bioturbation from a plant cover that developed on top of the limestone mainly after deposition. The horizontal cracks are interpreted as desiccation cracks that developed during short and/or repetitive periods of subaerial exposure and finally the desiccation of the lake. The root bioturbation and desiccation cracks lead to the formation of palustrine limestone. The cross-stratification and undulating character, mainly in the lower part of the limestone beds, are indicative of flowing water. In contrast, the abundant presence of complete charophyte stems is indicative of a low-energy environment and shallow water depth (Cohen & Thouin, 1987; Platt & Wright, 1991; García, 1994). The establishment of a shallow lake on the distal alluvial plain of a fan system could account for the reduced conditions leading to green-coloured clayey sediment in the top part of the mudstone in a basic cycle (Eardley *et al.*, 1973; Broekman, 1983; Abdul Aziz *et al.*, 2004). Alternatively, the green colour could be the result of reducing conditions during the deposition of the mudstone (Sagri *et al.*, 1989). According to Broekman (1983), the fine-grained organic matter is of allochtonous origin and was deposited on the lake shoreline during the transition from floodplain to lake depositional environment and vice versa. This interpretation is followed here, because the occasionally found horizontal laminations might indicate transportation of plant material into the basin. The organic material possibly was derived from the vegetation cover along the lake margin, which was washed into the basin during transgressive and regressive periods. Wetter climate conditions may have caused

higher lake levels during limestone deposition and this may have enhanced vegetation growth that, in turn, reduced the inflow of clastic material further into the basin (Broekman, 1983; Platt & Wright, 1991).

SEDIMENTOLOGY – MICROFACIES ANALYSIS

A detailed petrographic analysis of the limestone beds was performed to reconstruct duration and stability of lake expansions and water depth. Outcrop-scale description of the carbonate facies provides a rough estimate of these lake variables and the subsequent use of microfacies permits analysis of larger scale variations within these dynamic lake features. Carbonate petrography was carried out on a total of 145 thin sections from all 34 limestone beds in the Cascante section (Fig. 4). The limestone beds were sampled at a resolution of at least one thin section per 10 cm. To increase the visibility of carbonate particles, especially bioclast remains, the thin sections were partly stained using the red staining method of Lindholm & Finkelman (1972).

The microfacies analysis resulted in a grouping based on petrographic features and textures. Two main microfacies groups and eight sub-groups were differentiated (Table 1). The first group includes limestone beds showing microfacies typical of a shallow permanent lake environment, whereas the second group includes carbonate deposits showing features characteristic of a very shallow, transient (*sensu* Currey, 1990) lake environment. Currey (1990) defines transient lakes as having an inundation to desiccation time ratio of around 1:1, whereas permanent lakes have a ratio of over 1000:1. Letter labels for microfacies sub-groups were arbitrarily chosen. Thin sections that show characteristics in between two sub-groups were labelled as intermediate between the two sub-groups. Limestone beds consequently were labelled according to the microfacies code indicative of the deepest and most permanent lake environment recorded within the bed.

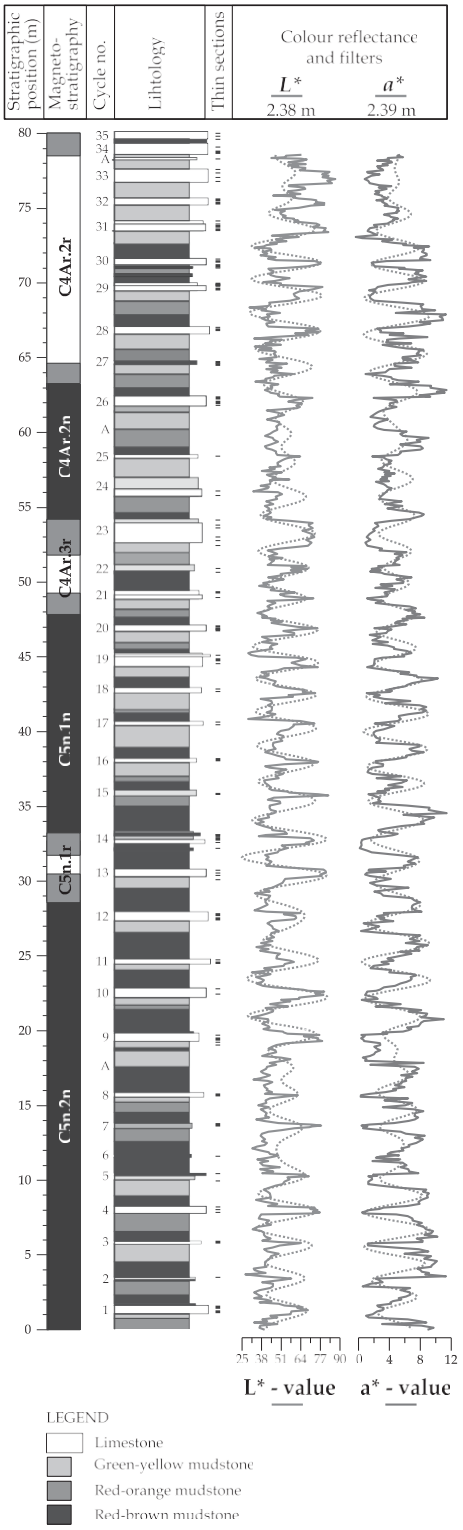

Fig. 4. Lithologic column and magnetostratigraphy of the Cascante section. Grey shading in the polarity record represents uncertainty intervals between samples with certain polarity. Grey shades in the lithological column represent colour differences, see legend. Basic mudstone–carbonate cycles are numbered to the left of the column. Location of limestone samples collected for thin sections is also indicated. The graph is completed by a* (red) and L* (blue) colour reflectance records and their 2Æ38 and 2Æ39 m filters (dotted lines) (modified from Abdul Aziz *et al.*, 2004).

Table 1. Specification of petrographic description, matrix, and bioclast characteristics of the eight carbonate microfacies sub-groups recognized in the Cascante section.

Group	Sub-group	General characteristics (classification according to Dunham, 1962, and Folk, 1959)	Micrite Concentration	Lamination	Primary gypsum	Burrows/roots	Sorting	Diversity	Orientation	Fragmentation	Concentration	Net water budget during deposition (interpretation) low high
Shallow *permanent lake* microfacies	**S**	Packstone and biomicrite. Charophyte stems, gyrogonites, ostracods and bivalves.	-	++	- -	- -	++	+	++	++	++	
	R	Wackestone and biomicrite. Ostracods, gastropods, charophyte stems, gyrogonites and bivalves. Some clotted micrite + fenestral features.	+	+	-	- -	+	+/-	+	+	+	
	Q	Wackestone and biomicrudite. Ostracods and charophytes. Clotted micrite and fenestral fabrics.	++	+/-	+/-	- -	+		+/-	+/-	-	
Very Shallow *transient lake* microfacies	**A**	Packstone, biomicrite or biomicrudite. Charophytes and gyrogonites, few gastropods, bivalves and thin ostracods.	- -	- -	- -	-		++	+/-	+	++	
	B	Wackestone and biomicrite. Bioclasts same as in A.	+/-	- -	-	+/-	+	+	+	+/-	+	
	C	Wackestone and biomicrite. Gastropods, some charophyte stems, gyrogonites and some ostracods.	+/-		+/-		+/-	+/-	+/-		-	
	D	Wackestone and biomicrite to biomicrudite. Some quartz grains and organic matter.	+/-		+	+	+/-	-	-		- -	
	E	Mud to wackestone and biomicrite. Ostracods and some gastropods and bivalves. Organic matter and peloids. Intraclast character. Some quartz grains.	++	- -	++	++	- -	- -	- -	++	- -	

No sign indicates lack of specific behaviour, +/) indicates average property with respect to the other microfacies, and + ()) stands for higher (lower) than average. To the right a schematic interpretation is given in terms of net water availability, see text for explanation.

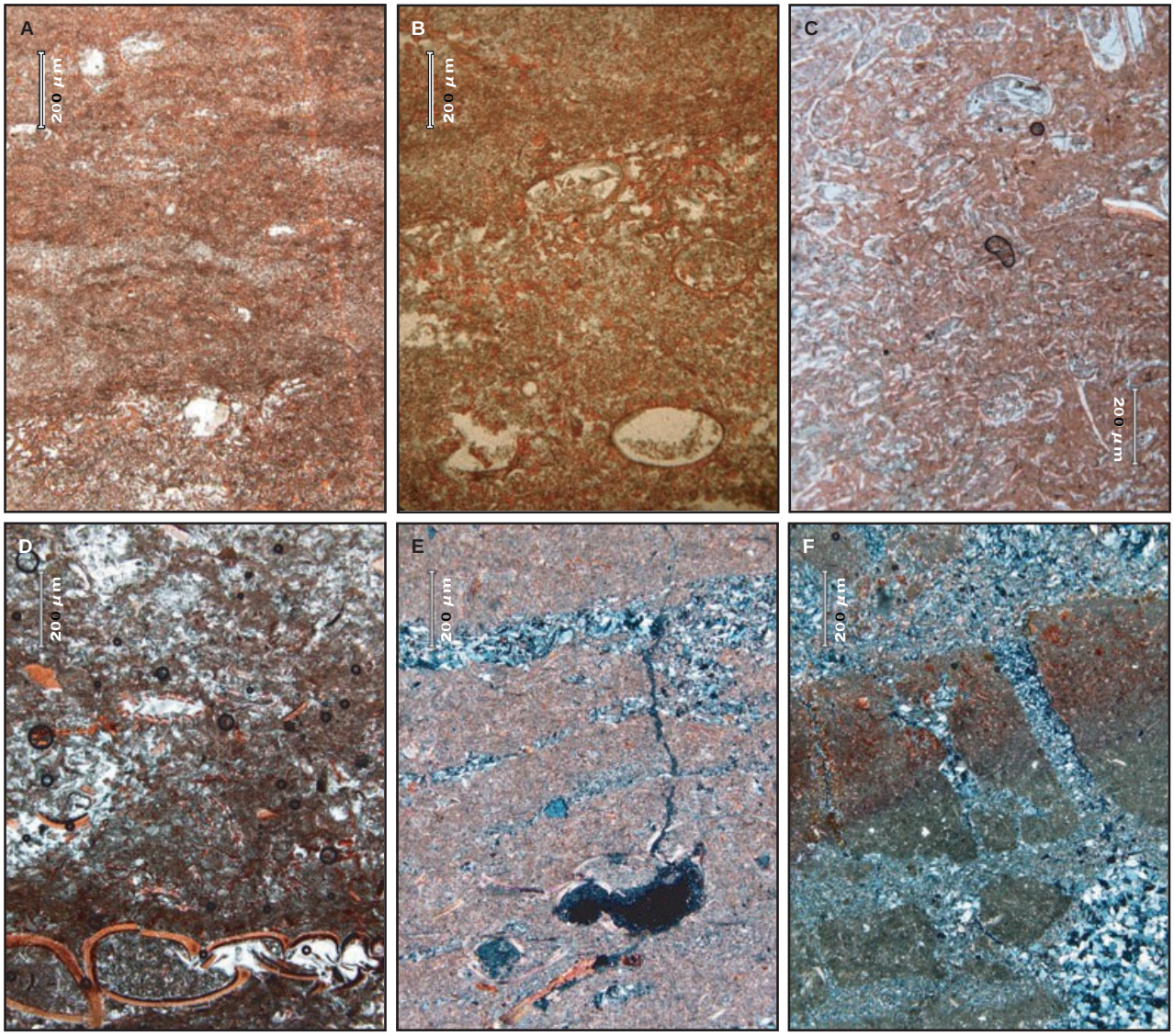

Fig. 5. (A) Example of *permanent lake* microfacies sub-group R showing lamination of micrite and broken remains of charophyte stems and gyrogonites that were transported to (slightly) deeper lake environments, normal polarized light. (B) Example of *permanent lake* microfacies sub-group Q showing lamination of dense micrite and both broken and complete charophyte remains indicative for only short transportation, red stained section, normal polarized light, scale as on other photomicrographs. (C) Example of *transient lake* microfacies sub-group A a high concentration of charophyte stems that shows a slight orientation, some gastropod remnants are present, the completeness of delicate charophyte remains indicative for low-energy environments without much transportation before deposition, section red stained, normal polarized light. (D) Example of *transient lake* microfacies sub-group C showing a relatively high concentration of broken and complete bioclast remains of mainly gastropods, red stained section, normal polarized light. (E) Example of *transient lake* microfacies sub-group D showing broken gastropod and ostracod shell remains, (primary) lenticular gypsum occurs as filling of horizontal desiccation cracks, red stained section, cross-polarized light. (F) Example of *transient lake* microfacies sub-group E showing microbreccia with host rock and filling of cracks with micrite and gypsum, palustrine limestone, upper half red-stained, cross-polarized light.

Shallow permanent lake microfacies

Description

The carbonate microfacies representative of shallow, permanent lake conditions include sub-groups Q, R and S (Figs 5A,B and 6A). These sub-groups show a dense packing of carbonate micrite and bioclast fragments and, from sub-group Q to R to S, an increase in sub-millimetre-scale lamination of micrite and

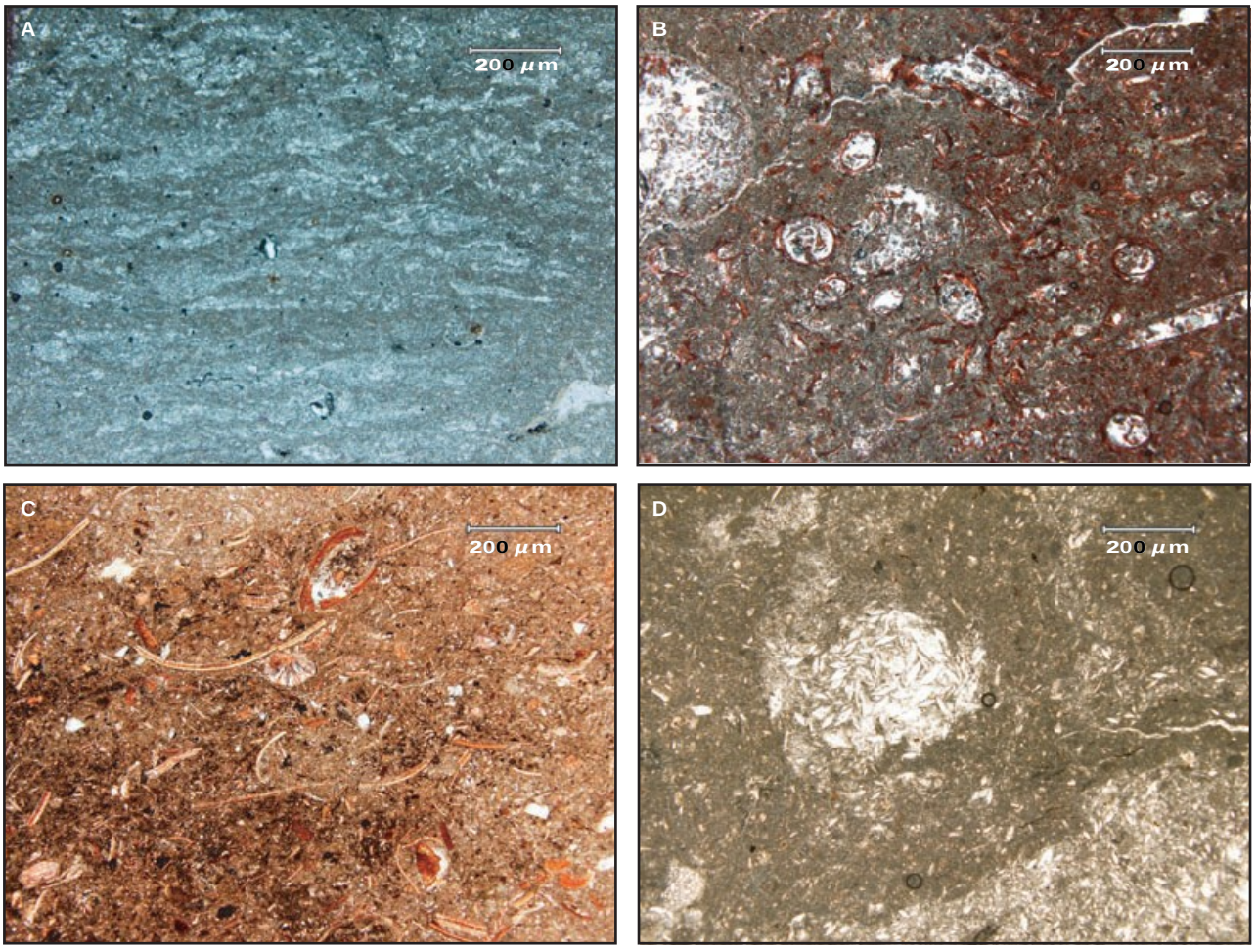

Fig. 6. (A) Example of *permanent lake* microfacies sub-group S lamination of micrite and broken remains of charophyte stems and gyrogonites transported to (slightly) deeper lake environments, normal polarized light. (B) Example of *transient lake* microfacies sub-group B showing abundant and mostly complete charophyte remains indicative of low energy conditions, no preferred orientation of micrite or bioclasts, some signs of sub-aerial exposure and/or root action in upper part of photograph, section red stained, normal polarized light. (C) Example of *transient lake* microfacies sub-group C/D showing gastropod and unidentified shell remains at intermediate densities without clear orientation and organic matter, section red stained, normal polarized light. (D) Root burrow or striotubule filled with lenticular gypsum, host rock around burrow shows primary lenticular gypsum as well, not red stained, normal polarized light.

bioclast fragments. Bioclast diversity and fragmentation, as well as packing of the bioclast fragments, increase from sub-group Q to S ('concentration' in Table 1). Bioclasts consist mainly of fragmented charophyte stems and gyrogonites and minor ostracod and gastropod shells, which are present chiefly in sub-group Q (Fig. 5B). None of the three sub-groups contains siliciclastic material coarser than the mud fraction, whereas clay material is present in minor amounts. No cracks and burrows have been observed, nor gypsum crystals. On outcrop scale, the limestone beds of this microfacies are indurated and have a well-defined base and top. Beds are internally laminated to massive; small-scale cross-stratification and undulating structures are common, especially in the basal part of the beds. Bed thickness ranges from 0·4 to 0·9 m.

Interpretation

The dense packing of micrite and bioclast fragments and the sub-millimetre-scale laminations are interpreted as the result of deposition in relatively low-energy water environments. Lenticular gypsum, that is interpreted as primary gypsum by Anadón *et al.* (1992), is present abundantly in the *very shallow transient* microfacies. The absence of cracks, burrows and lenticular gypsum in the *shallow permanent lake* microfacies indicates stable lacustrine conditions

that prevailed for relatively long time periods (Currey, 1990). The abundance of fragmented charophyte stems and gyrogonites suggests that they were transported over a short distance from very shallow lake areas, where charophytes flourished, towards slightly deeper waters (Platt, 1989; Pérez *et al.*, 2002). Platt (1989) and Pérez *et al.* (2002) state that water depth in these environments probably does not exceed a few metres. Stable lacustrine conditions prevail when evaporation and groundwater discharge from the lake system are lower than precipitation and groundwater influx. These circumstances may be related to relatively continuous water inflow, together with low evaporation, and/or lack of extremely dry climatic conditions for a certain period of time. The increase in horizontally oriented bioclasts, clast fragmentation, and micrite and bioclast lamination from sub-group Q to S is interpreted as slightly higher energy and deeper conditions towards sub-group S. No microfacies are observed that indicate the deeper and less energetic settings that are expected when lake levels rise even more; this means that in the case of Cascante the 'deepest' observed lake is also the relatively highest energy environment probably indicating a shallow lake environment with a flat bottom.

Very shallow transient lake microfacies

Description

Limestones of this microfacies consist of massive, uniform carbonate micrite lacking lamination (microfacies A to E) and scarcely containing very fine sand-sized quartz grains (see also Freytet & Verrecchia, 2002). The distinction between sub-group Q (a microfacies typical of deposition in shallow permanent lake conditions; Fig. 5B) and sub-group A (Fig. 5C) is based primarily on the absence of lamination and reduced packing of micrite in sub-group A. From sub-group A to E, a decrease in diversity and packing of bioclasts is observed (Figs 5C to F and 6B,C; Table 1). Charophyte stems and gyrogonites prevail in sub-groups A and B (Figs 5C and 6B), while many complete and some broken ostracod and gastropod shells are more common in sub-groups D and E (Fig. 5E and F). In sub-group C (Fig. 5D), all four types of, dominantly broken, bioclasts are present, although they are often not well-mixed. An increase in the amount of sub-millimetre-sized particles of organic matter, most probably derived from plant material, can be observed from sub-group C to D (Figs 5D, E and 6C). Sub-millimetre-sized lenticular gypsum crystals occur often floating in the carbonate micrite, with their presence increasing from sub-group B to E.

Limestone beds showing this microfacies group usually display mainly horizontal and some vertical cracks (Fig. 5E and F), and vertical burrow (striotubules) structures (Fig. 6D). The burrows become significantly more abundant from sub-group A to E. Horizontal cracking and bioturbation features are virtually absent in sub-group A, while in sub-group E brecciation is intense (Fig. 5F). Cracks commonly are filled with a mosaic of lens-shaped sub-millimetre-scale gypsum crystals but, in some cases, they are filled partially with silt-sized to clay-sized siliciclastic material or fragmented host carbonate rock, the latter especially in desiccation breccia (*sensu* Normati & Salomon, 1989) of sub-group E. The sub-groups B, C and D show gradational microfacies features between the two end-member sub-groups A and E.

In outcrop, the carbonate beds displaying *very shallow transient lake* microfacies usually are massive and/or poorly laminated and frequently intercalate with thin green clay and dark grey organic-rich mudstone beds that have a thickness between 1 and 10 cm.

Interpretation

The lack of lamination in all sub-groups, minor amounts of gypsum and abundant well-preserved charophyte cysts and stems, and gyrogonites in this microfacies indicates a very shallow, low-energy freshwater lake environment. The delicate charophyte stems grow in shallow lake margins and usually break apart when agitated and transported, as observed in modern lake environments, where meadows of charophytes flourish at depths of less than 5 m (Platt, 1989; García, 1994; Pérez *et al.*, 2002).

The decrease in abundance and diversity of bioclasts and the increased organic matter and amount of root burrows in the limestone, as observed from sub-group A to E, indicate a gradual change from a low energy, shallow lake environment (sub-group A; Fig. 5C) towards a shallow lake environment that is more swampy. This interpretation is supported by the increase in lenticular gypsum floating in the carbonate micrite from sub-group A to E. Anadón *et al.* (1992) relate similar lenticular gypsum crystals to a primary evaporate phase in extremely shallow lake environments, even though Albesa *et al.* (1997) report that the salinity is not necessarily high. The higher amount of horizontal cracks, that

are interpreted as desiccation cracks, and root burrows (striotubules) observed from sub-group A to E, suggests an increase in frequency and duration of sub-aerial exposure (sub-group E in Fig. 5F). Alonso Zarza (2003) states that the absolute exposure time and frequency needed to form palustrine features in freshwater lake carbonate deposits are not known and may be relatively short, even a season. The primary exposure features can form under fluctuating lake water level, which is accompanied by deposition of organic plant material and clay laminae intercalated in the limestone bed. In terms of inundation versus exposure time, carbonate microfacies sub-groups A and B characterize a 'persistent' lake environment, suggesting an inundation versus desiccation ratio of 10 to 1000:1 (Currey, 1990), while microfacies sub-groups C to E represent a 'transient' lake environment, with a ratio of 1 to 10:1. Limestone beds of the *very shallow transient lake* microfacies sub-groups generally show their relatively deepest lake phase just above the middle of the bed.

PALAEOENVIRONMENTAL CYCLES

Sedimentary model for the basic cycle

The remarkable lateral continuity of lithologic features of both mudstone and limestone beds in the Cascante succession suggests that they were deposited in a low-energy, endorheic ramp-type basin. In this setting, small-scale lake-level fluctuations resulted in the submergence or desiccation of large areas of the basin (Platt & Wright, 1991). The description and interpretation of the basic mudstone–limestone sedimentary cycle are schematically depicted in Fig. 3. It should be noted that the mudstone part of the cycle is on average three to four times thicker than the limestone interval. Within the basic cycle, red mudstone is interpreted as a low-energy sheet flow deposit that underwent sub-aerial exposure after deposition in a distal alluvial plain setting. The transition from a red to a greenish colour towards the top of the mudstone deposit most probably is caused by reduction and leaching of the underlying muddy sediment when lake levels rose following mudstone deposition. Organic-rich layers below and on top of the lacustrine limestones are interpreted as deposited during the lake transgression and regression. The freshwater limestone is associated with lake-level highstands resulting in a shallow lake undergoing varying scales of fluctuating lake levels. In some cases, low lake levels resulted in episodic exposure of the carbonate mud and the formation of palustrine features. Lack of significant siliciclastic input into the carbonate lake can be related to high lake levels, resulting in a rise of the base level of erosion trapping the sediment in higher areas (Picard & High, 1981), and/or to the development of a dense vegetation cover along the lake margin that kept sediments in place and promoted chemical instead of physical weathering (Platt & Wright, 1991).

Larger-scale environmental variations

The codes of the different microfacies sub-groups for the 34 limestone beds in the Cascante section have been plotted in Fig. 7. Carbonate microfacies characteristics of *very shallow transient lake* environments prevail in the lower part of the section below cycle 26. Two intervals with three basic cycles (10 to 12 and 15 to 17) and one interval with two cycles (20 and 21) contain limestones representative of more 'persistent' (see above) lake environments (sub-groups A and B). Except for cycle 4, all other limestones in the lower part of the section show more 'transient' lake environments (i.e. palustrine limestones of sub-groups C, D and E) representing shallower and more variable lake conditions. Below cycle 26, no limestone bed with microfacies indicative of *shallow permanent lake* conditions is present. Above that cycle, the limestone beds comprise microfacies sub-groups that indicate the more persistent environments of the *very shallow transient lake* microfacies (sub-groups A and B) and the permanent environments of the *shallow permanent lake* microfacies (sub-groups Q, R and S), except for cycle 27. Thus, lake levels increase and lake environments become more stable from cycle 26 onwards, probably indicating the transition to the thick lacustrine limestone unit that overlies the studied section. This uppermost interval is

Fig. 7. Microfacies analysis results of all limestone beds in the Cascante section and their correlation to successive precession minima and insolation maxima according to the magnetostratigraphy of Hüsing *et al.* (2007). Grey in the polarity record indicates age uncertainty intervals as given by these authors. Colours and different line characteristics indicate microfacies sub-groups (see legend). Asterisks indicate thick mudstone intervals. For details on the lithological column see Fig. 4.

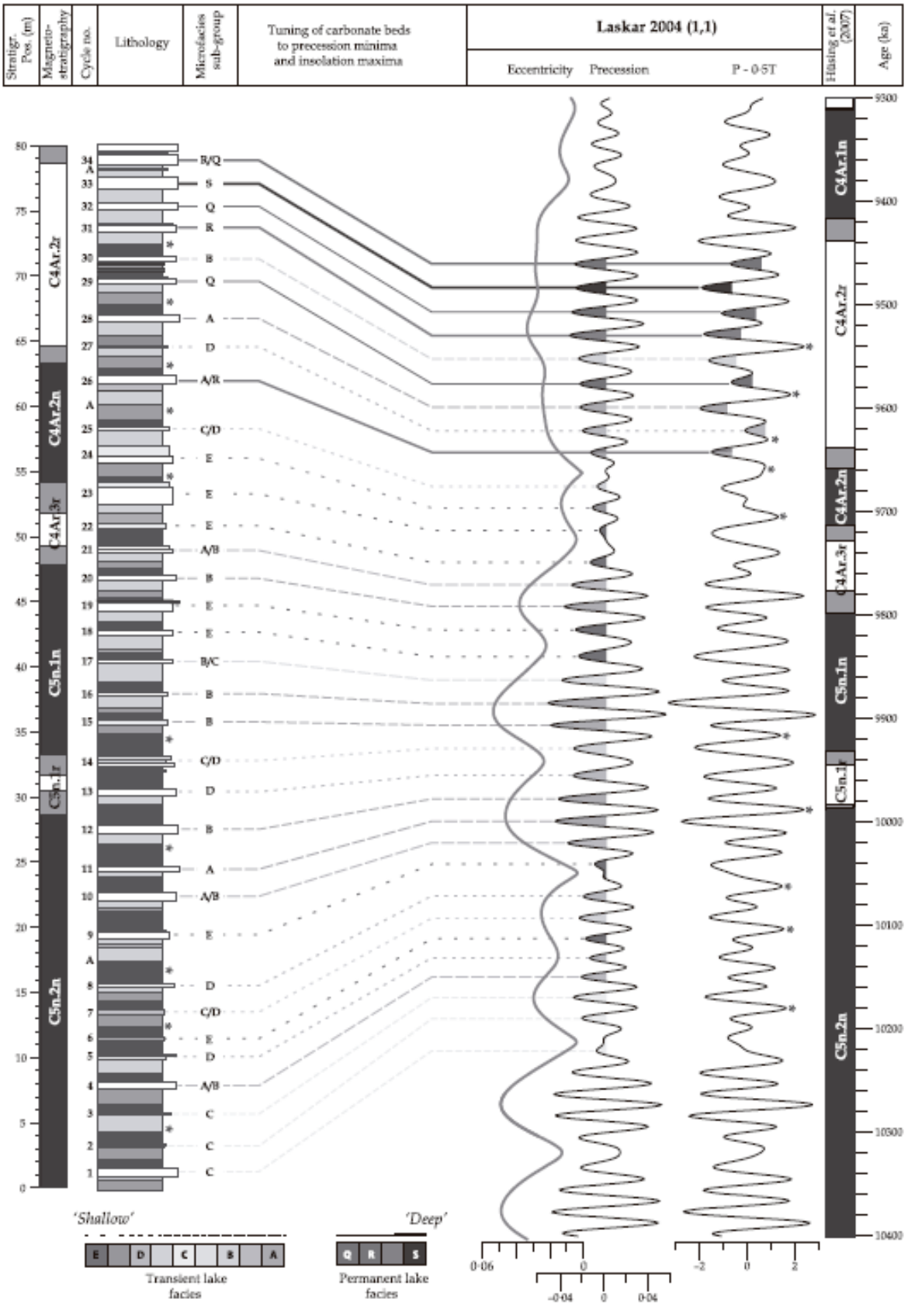
Stratigr. Pos. (m)
Magneto-stratigraphy
Cycle no.
Lithology
Microfacies sub-group
Tuning of carbonate beds to precession minima and insolation maxima
Laskar 2004 (1,1)
Eccentricity
Precession
P - 0·5T
Hüsing et al. (2007)
Age (ka)
C4Ar.2r
C4Ar.2n
C4Ar.3r
C5n.1n
C5n.1r
C5n.2n
'Shallow'
'Deep'
E D C B A
Q R S
Transient lake facies
Permanent lake facies

characterized by alternation of relatively deeper and shallower lakes in every other bed. This pattern shifts one cycle from 28 to 29. Somewhat deeper lakes are found in cycles 26, 28, 29, 31 and 33, whereas shallower lakes are found in cycles 27, 30, 32 and 34.

CYCLOSTRATIGRAPHY

Astronomical forcing

The stratigraphic regularity of the basic cycle in the Cascante section strongly suggests an allocyclic forcing mechanism. Abdul Aziz *et al.* (2004) therefore applied Blackman–Tukey (BT) and maximum entropy (ME) spectral analysis on colour reflectance records (Fig. 4) in the depth domain. The dominant peak in the resulting power spectra could be related to the basic, 2Æ2 m cycle. Additional power was found at lower frequencies, with a thickness ratio of about 1:2:5. This ratio closely corresponds to the astronomical period ratio of climatic precession, obliquity and short (*ca* 100 kyr) eccentricity (Abdul Aziz *et al.*, 2004). Detailed age control in the section was derived from the magnetostratigraphy (Fig. 4) calibrated to the geomagnetic polarity timescale CK95 using mammal biostratigraphic data (Abdul Aziz *et al.*, 2004). Application of this age model revealed a period of 20 to 26 kyr for the basic cycle. This period is well within the range of the duration of the climatic precession cycle. The other peaks identified by the spectral analysis indicate a period of *ca* 41 kyr for the cycle with a thickness twice that of the basic cycle and around 100 to 150 kyr for the cycle with a thickness of five times the basic cycles. These cycles are tentatively related to obliquity and the *ca* 100 kyr period of the short eccentricity cycle. Abdul Aziz *et al.* (2004) concluded that these results strongly indicate that the sedimentary cyclicity in the Cascante section is related to astronomical forcing. The use of the recently improved astronomical tuned timescale (Lourens *et al.*, 2004) and the astronomical ages resulting from the tuning of the deep marine Monte dei Corvi section (Hü sing *et al.*, 2007) does not change the outcome of the statistical analysis.

The potential astronomical control requires further exploration. In order to elaborate on this, the sedimentary cycles need to be interpreted in terms of astronomical climate forcing. Once the phase relationships have been established, an astronomical tuning of the sedimentary cycles by correlation of individual cycles to calculated astronomical target curves can be constructed starting from the magnetostratigraphic age calibration. Finally, the environmental interpretations derived from the carbonate microfacies analysis can be compared with the target curves and the working hypothesis can be examined. This cyclostratigraphic exploration does not imply that alternative interpretations of the cyclicity are excluded. However, the data strongly suggest orbital forcing and this option has been elaborated to (finally) prove astronomical forcing using an integrated approach.

Climatic interpretation of the sedimentary cycles

The alternation of shallow lake and distal alluvial plain facies indicates constant shifts at 10^4 year timescales between an annual or seasonal net positive and negative water budget, when the basic cycles are interpreted as forced by climate variations. From the sedimentological data alone, it is impossible to deduce whether these variations were caused by changes in precipitation, evaporation, seasonality, rain season and/or possibly other climatic factors. Horizontal desiccation cracks and root traces, which increase towards the top of the carbonate beds, indicate that lake levels often were variable and high lake levels only prevailed for a short period of time. Lake-level fluctuations resulted in rapid drowning or desiccation of the depositional site. The weak development of palustrine features indicates that sedimentation resumed not long after the ending of lake conditions, as palustrine features can form rapidly in *ca* 10^1 to 10^3 years (Alonso Zarza, 2003). The amount of time represented by the limestone versus mudstone part of the basic cycle is difficult to specify. The lack of well-developed pedogenic features in the mudstones suggests that sedimentation kept pace with soil formation processes within the mudstones (Buurman, 1980). Sedimentation was apparently relatively continuous during both the deposition of the mudstone and limestone part of the basic cycle. However, major differences in the sedimentation rate between the two end-member lithologies may exist. In conclusion, the observed regular and repetitive development of full lacustrine conditions in a prevailing subaerially exposed distal floodplain requires a cyclic forcing mechanism to yield a positive water budget during specific and relatively short time periods.

Phase relationships – geological data

Correlation of individual mudstone and carbonate cycles with calculated astronomical target curves requires a knowledge of the phase relationship of the two basic cycle end-member lithologies with the orbital parameters. Consequently, the climatic influence in terms of net water budget of orbital extremes and, additionally, the climatic conditions required for development of the depositional environments of mudstone and limestone have to be unravelled. This rationale is termed phase relationship between lithology and orbital parameters.

In the northern hemisphere, climatic precession minima (summers in perihelion) cause high summer and low winter insolation at the top of the atmosphere resulting in enhanced seasonality. Numerous studies have demonstrated the influence of precession on circum-Mediterranean climate as recorded by Neogene marine (Rossignol-Strick, 1983; Hilgen *et al.*, 1999; Foucault & Mélières, 2000) and continental sediments (Steenbrink *et al.*, 1999; Abdul Aziz *et al.*, 2000; Magri & Tzedakis, 2000). Increased clay contents in cyclic Pliocene marl sequences deposited offshore Gulf of Cadiz suggest higher annual runoff from a southern Spanish drainage area at times of precession minima (Sierro *et al.*, 2000). Similarly, indications for humid conditions during precession minima have been implied for marl sequences of the Abad Formation in the Sorbas Basin in southern Spain (Sierro *et al.*, 1999; Vázquez *et al.*, 2000). Sapropel formation in the eastern and western Mediterranean basins has been related to increased winter precipitation from southern, and possibly northern, Mediterranean borderlands during precession minima (Lourens, 2004). Magri & Tzedakis (2000) reported temperate-stage forest expansions during boreal summer insolation maxima (during precession minima) for the last 200 kyr in central Italy, which they relate to higher annual net precipitation. Maximum forest coverage occurs during autumn insolation maxima, which Magri & Tzedakis linked to the absence of extreme summer evaporation and, consequently, to maximum net water budget. On the other hand, a significant contraction of the forest coverage is found during winter insolation maxima (i.e. summer insolation minima during precession maxima) and March insolation maxima.

Reduced clastic supply that resulted in marl-rich intervals in the Pliocene Gulf of Cadiz is observed during short and long eccentricity minima (Sierro *et al.*, 2000). Moreover, intervals devoid of sapropels in the Mediterranean occur during eccentricity minima and are related to lower precipitation in the southern, and possibly northern, borderlands (Lourens, 2004). Short (*ca* 100 kyr) and long (405 kyr) eccentricity minima most probably result in prolonged periods of relatively dry climate conditions that can lead to lake-level lowstands in the Spanish mainland.

Phase relationships – climate modelling

In order to determine the impact of climatic precession extremes on climate in Spain, model simulations were performed by using an atmospheric global climate model of intermediate complexity, SPEEDY, coupled to a slab ocean and a simple land model. SPEEDY is a primitive equation model with simplified physics parameterizations (Molteni, 2003) that has a horizontal resolution of about 3Æ75° · 3Æ75° (T30) and seven vertical levels (Hazeleger *et al.*, 2003). The land model consists of a simple bucket model, which implies that the soil moisture cannot exceed 15 cm per grid box. Redundant soil moisture is defined as runoff. Three 100 year simulations using the SPEEDY climate model were carried out: (i) a control run with present-day orbital parameters; (ii) a minimum precession run (eccentricity = 0Æ056, precession =)0Æ055); and (iii) a maximum precession run (eccentricity = 0Æ058, precession = 0Æ058). A precession maximum (minimum) means winter (summer) solstice in perihelion. Precession is defined as $e \sin(\varpi + \lambda)$ with e the eccentricity of the orbit of the Earth and λ the angle between the vernal equinox and perihelion (measured counter-clockwise). The used values for precession are the extreme values occurring in the last one million years (Berger, 1978). For the precession simulations, obliquity was kept fixed at 22Æ08, *i.e.* the minimum value for the last one million years. A fixed obliquity was used to focus on the precession signal without the possible interference of obliquity. For all three runs, boundary conditions such as orography, concentration of trace gases, vegetation and ice sheets were kept to present-day values. A more extensive description of the experimental set-up can be found in Tuenter *et al.* (2003). The model results are shown as averages over the last 10 years of 100 year simulations. Ten years are used to average out annual variability, while a longer averaging period is not used to ensure that the model is in equilibrium after 90 years.

The model shows that during winter, net precipitation (precipitation minus evaporation) in precession minimum is higher than in precession maximum (Fig. 8C) while, for summer, there is not much difference between the precession extremes. The large difference in net winter precipitation is caused by stronger precipitation during minimum precession, whereas winter evaporation is equal for both minimum and maximum precession (Fig. 8B). In the model, the reason for enhanced winter precipitation during precession minima is higher Mediterranean sea surface temperatures both in summer and in winter. These higher temperatures are due to increased summer insolation which, in the winter, results in higher evaporation and formation of clouds over the Mediterranean. In summer, higher precipitation occurs during maximum precession (Fig. 8A), although summer net precipitation is similar for both precession extremes (Fig. 8C) because of an increase in evaporation (Fig. 8B). Annually, higher net precipitation occurs during minimum precession (Table 2).

In the model, the annual net precipitation is dominated by winter precipitation for both minimum and maximum precession, suggesting that winter precipitation plays an important role in runoff and groundwater supply that together determine lake levels. Runoff acts accordingly with higher winter and annual runoff during precession minima (Fig. 8D; Table 2). Therefore, it is probable that high lake levels and carbonate deposition in the Cascante section occurred during precession minima.

The phase relationship of high lake levels during precession minima derived from the SPEEDY model are in line with the sedimento-

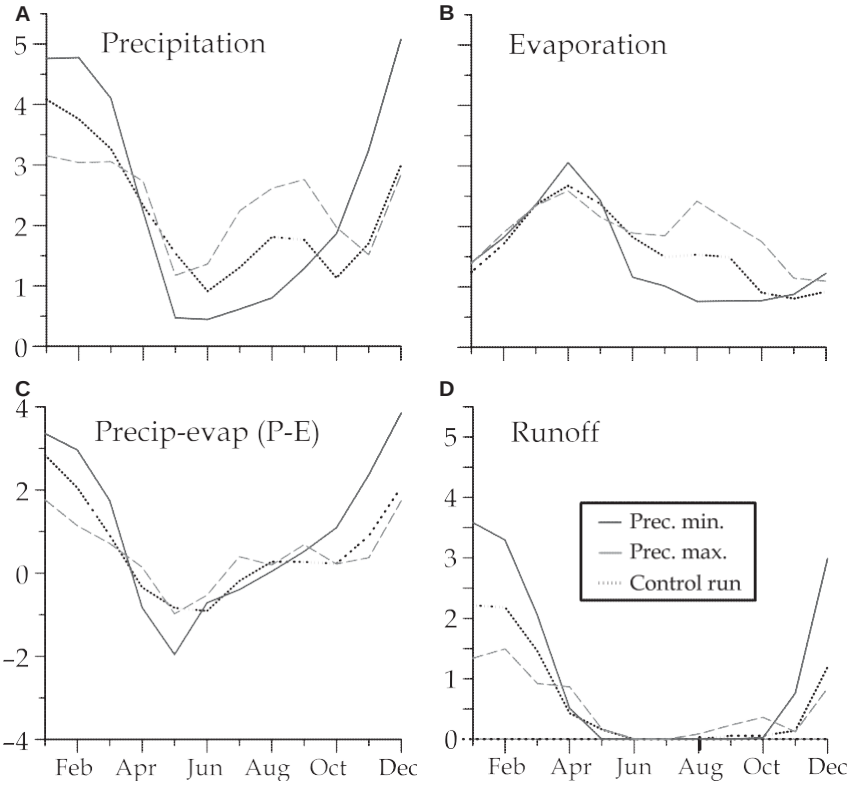

Fig. 8. (A) to (D) Monthly area averaged values for 'Spain' (10Æ5 to 2° W; 37 to 44Æ5° N, four gridboxes) of: (A) precipitation; (B) evaporation; (C) precipitation minus evaporation; and (D) runoff for the control run (dotted black line), minimum (climatic) precession run (solid line) and the maximum precession run (dashed line). All values are in mm day^{-1} and averages of the last 10 years of 100 year simulations (see text for details).

Simulated annual values	Precipitation (mm day^{-1})	Evaporation (mm day^{-1})	Precip.–Evap. (mm day^{-1})	Runoff (mm day^{-1})
Control run	2Æ22	1Æ61	0Æ61	0Æ66
Precession min.	2Æ47	1Æ47	1Æ00	1Æ10
Precession max.	2Æ37	1Æ88	0Æ49	0Æ54

All values are averages of the last 10 years of 100 year simulations.

Table 2. Annually averaged values for 'Spain' (10Æ5 to 2° W; 37 to 44Æ5° N, four gridboxes) of precipitation, evaporation, precipitation minus evaporation (net precipitation), and runoff for the control run, minimum precession, and maximum precession.

logical findings in the Gulf of Cadiz (Sierro *et al.*, 2000) and the Sorbas Basin (Vázquez *et al.*, 2000) as well as those from sapropelic layers in the Mediterranean (Lourens, 2004). Moreover, the results agree with forest expansions during precession minima (Magri & Tzedakis, 2000). Considering the geological and modelling data, the phase relationship between high lake level (and limestone formation) and enhanced net winter precipitation during precession minima is favoured.

Astronomical Tuning

An astronomical tuning is constructed for the Cascante section using the astronomical ages for the reversal boundaries of Hüsing *et al.* (2007) and the inferred phase relationships between the carbonate beds to minimum precession and mudstone beds to maximum precession, as discussed above. The astronomical tuning is established by correlating the basic cycles to the precession target curve of Laskar *et al.* (2004) starting from all the reversal boundaries upwards and downwards (Fig. 7). Except for the base of chron C5n.1r, which is *ca* 10 kyr younger in Cascante, the tuning produces similar astronomical ages for chron boundaries as calculated by Hüsing *et al.* (2007). This observation implies that exactly the same number of precession-related cycles is present in the Cascante section as in the time-equivalent interval in the Monte dei Corvi section. This outcome confirms the astronomical forcing and dominant precession control of the basic cyclicity at Cascante.

As described above, the microfacies analysis revealed larger scale lake-level variations comprising several basic cycles. Lowstands therein, with beds showing features indicative of the shallowest *transient lake* environment (microfacies sub-groups C, D and E; cycles 1 to 3, 5 to 6, 7 to 9, 13 to 14, 18 to 19 and 22 to 25), correlate to minimum eccentricity related to the *ca* 100 kyr cycle (Fig. 7). Highstands with beds that formed in the relatively deeper *transient lake* environment (microfacies sub-groups A and B; cycles 4, 10 to 12, 15 to 17 and 20 to 21) were deposited during maxima of the short eccentricity cycle. The prolonged lowstands (cycles 1 to 9 and 22 to 25) correspond to long (405 kyr) eccentricity minima and prolonged highstands (cycles 10 to 21 and 26 to 34) to long eccentricity maxima (Fig. 7). This link between lake level, as derived from microfacies analysis, and eccentricity indicates that the eccentricity modulation of the precession amplitude played an important role in determining longer-term variations in lake level. The observed lake-level lowstands during short and long eccentricity minima are in line with the modulating effect of eccentricity and with Mediterranean marine geological data (Sierro *et al.*, 2000; Lourens, 2004).

In the interval above cycle 25, successive limestone beds display an alternation of deeper and shallower lake carbonate deposits (Fig. 7). Moreover, the mudstone beds reveal a regular alternation in this interval; successive mudstones show a thick and thin alternation while red colouring is present in the thicker beds (shown with an 'asterisk' in Fig. 7) and absent in the thinner beds (cycles 27 to 31 in Fig. 7). These kinds of alternations in basic precession controlled cycles are found in the marine realm as well, where thick pronounced and thin, vague sapropels alternate (Hüsing *et al.*, 2007). Such alternating patterns that occur superimposed on a basic precession-forced cyclicity are called precession–obliquity interference patterns. These patterns originate from interference of these two orbital parameters, which typically are found during times of low eccentricity when the precession amplitude is reduced. In particular, these patterns occur at times of minimum eccentricity related to the long-period 2Æ4 Myr eccentricity cycle (Abdul Aziz *et al.*, 2003a; Laskar *et al.*, 2004; Hüsing *et al.*, 2007). Precession–obliquity interference patterns have also been recognized in continental sediments (Abdul Aziz *et al.*, 2003a). The interference pattern in the Cascante section (cycles 26 to 34) indeed occurs during a minimum of the 2Æ4 Myr eccentricity cycle. This cycle reaches its absolute minimum at 9Æ52 Ma, which is the minimum in the 2Æ4 Myr bandpass filter of the eccentricity time series (Laskar *et al.*, 2004).

In the marine realm, the interference patterns in sapropel successions fit with those in the insolation target curves (Hüsing *et al.*, 2007). Such a fit can be used to confirm the astronomical tuning in these sensitive deep marine settings. In the Cascante section, the details in the interference pattern also fit with the combined precession–obliquity target curve (P–0.5T in Fig. 7). Deeper, more permanent lakes occur during extreme summer insolation maxima (P–0.5T minima) and thicker, more intense red mudstones during extreme summer insolation minima, which results from the additional influence of obliquity maxima and minima, respectively. This fit is consistent with the astronomical tuning of the Cascante section. In the lower part of the section,

interference patterns also are present, especially below cycle 9 (see Fig. 7). However, this is not further discussed in detail because the patterns are much less pronounced in this interval and an independent quantitative record is needed to prove the correlation. Nevertheless, there is a good fit with the interference patterns in P–0.5T in this interval as well.

In conclusion, the astronomical tuning of the Cascante cycles to the precession time series does not reveal any significant difference in the astronomical age of the magnetic reversal boundaries as compared with the astronomically tuned sapropel succession at Monte dei Corvi (Hü sing *et al.*, 2007). The larger scale lake-level variations, revealed by microfacies analysis, fit well with the eccentricity target curve as expected from Mediterranean marine geological data. Additionally, precession–obliquity interference patterns in the upper part of the section reveal a good fit with the insolation target curve. These results confirm the astronomical forcing working hypothesis of the sedimentary cycles in the continental Cascante section.

DISCUSSION

The integrated cyclostratigraphic study was carried out to explore further the astronomical forcing of sedimentary cyclicity in the Cascante section, as previously suggested by the results of spectral analysis of colour records (Abdul Aziz *et al.*, 2004). All data are now consistent with the astronomical forcing hypothesis, indicating that astronomical forcing is indeed the most probable mechanism.

Outcrop sedimentology, microfacies analysis, magnetostratigraphy and modelling results show that (all) palaeoenvironmental variations at 10^4 to 10^5 year timescales could be related to astronomically forced climate variations. The basic cycle is forced by the climatic precession cycle, whereas longer-term lake-level variations are related to the short and long eccentricity cycles. Obliquity influence is observed during periods of low eccentricity.

The dominance of astronomically forced environmental variations throughout the Cascante section implies that orbitally induced changes in insolation had a prominent imprint on climate in Spain during the Late Miocene. These variations are recorded, especially in low-gradient closed basin settings such as Cascante. Lake-level fluctuations could have been forced by various mechanisms, mainly tectonics, climate and autogenic processes. Based on the combined cyclostratigraphy and microfacies study of the Cascante section it is argued that tectonic, autogenic and local climate processes had no significant effect on the Cascante palaeoenvironment on 10^4 to 10^5 year timescales. From a tectonic point of view, basin subsidence and/or margin uplift apparently occurred at constant rates or at least the difference between the two factors remained similar on the 10^4 to 10^5 year timescales, such that recorded palaeoenvironmental changes at these timescales are exclusively related to orbital climate variations.

Gradual change

Different scales of lithological cyclicity in the Cascante section are ascribed to astronomical forcing. In theory, these astronomical signals can be subtracted from the record in order to examine whether other unexplained palaeoenvironmental variations exist in the Cascante section; however, this can strictly be done only by using quantitative records. The present proxies are not indicative of any variations on timescales of 10^4 to 10^5 years, that are not related to astronomical forcing. On longer timescales, a gradual shift from dominant *transient* to mixed *transient–permanent* lake environments is observed after cycle 25 (Fig. 7) culminating in the fully lacustrine limestone unit on top of cycle 34 (Fig. 2). Clearly, this shift cannot be explained by the astronomical cycles discussed before. The causes for this major shift can be tectonics, non-astronomical climate, astronomical climate forcing because of cycles with a longer period, or autogenic processes.

Million-year timescale changes, such as the shift to deeper and more permanent lake environments after cycle 25 in the Cascante section, commonly are related to tectonic processes. In the lacustrine record of the Triassic Newark Basin, large-scale lithological variations are interpreted to reflect long-period astronomical climate variations (Olsen & Kent, 1996). However, a decisive conclusion about the potential long-period orbital climate forcing in the succession studied by Olsen & Kent (1996) cannot be made because of insufficient absolute age control and lack of an astronomical target curve for the Triassic. In the Neogene, eccentricity and obliquity comprise long-period cycles of *ca* 2Æ4 Myr and *ca* 1Æ2 Myr, respectively (Laskar *et al.*, 2004). Recently, the influence of these quasi-cycles on temperature and precipitation of climate of the Iberian Peninsula has been suggested by their impact on

mammal turnover rates (Van Dam *et al.*, 2006). In particular, long-period eccentricity minima, that are successively 2Æ0 and 2Æ8 Myr apart, resulted in prolonged absence of extreme summer conditions leading to an increase in both wet-adapted small-mammal lineages and total diversity (Van Dam *et al.*, 2006). In Cascante, the shift above cycle 25 from transient lake environments in the wettest phase of the basic cycle to a mix of transient and permanent lake environments occurs at an eccentricity minimum of *ca* 2Æ4 Myr (Fig. 7), whereas the environmental effect is consistent with the results of Van Dam *et al.* (2006). This coincidence is tempting, although proof for such a link should come from the accurate dating of a number of such large-scale transitions, ideally in different basins. Note that the phase relationship with eccentricity would then be different for the *ca* 2Æ4 Myr cycle than for the much better known short and long eccentricity cycles.

CONCLUSIONS

In the Cascante section, high-resolution magnetostratigraphic age control, together with carbonate petrography and outcrop sedimentology, as environmental proxies, reveals that all palaeoenvironmental signals at 10^4 and 10^5 year timescales are related to astronomical climate forcing. Modelling results show, consistent with geological data, that lake-level highstands are related to higher net winter precipitation during precession minima. The robust astronomical tuning reveals that the longer-term lake-level highstands, as revealed by the microfacies analysis, occur during *ca* 100 kyr and 405 kyr eccentricity maxima, as a consequence of the modulation of the precession amplitude. Subtracting the astronomical signals from the palaeoenvironmental variation in the Cascante section revealed a shift towards deeper and more permanent lake environments at times of precession minima in the upper part of the section. This shift, which culminates in a thick lacustrine limestone unit on top of the studied section, remains unexplained, but may be triggered by tectonics, non-astronomical climate change, astronomical climate forcing because of very long period cycles, and autogenic processes.

In summary, the results illustrate that cyclostratigraphy is a powerful tool to study palaeoenvironmental variations in continental successions at timescales greater than 10^3 years. Astronomical climate forced variability can be constrained very well, if sufficient age control and palaeoenvironmental proxies are present. Such a detailed study can be especially useful in Late Neogene successions, for which the geomagnetic timescale has been improved considerably by the incorporation of astronomically tuned reversal ages (Lourens *et al.*, 2004; Hüsing *et al.*, 2007).

ACKNOWLEDGEMENTS

Jesus Sanchez-Corral from the Universidad Complutense de Madrid and Otto Stiekema from Utrecht University are thanked for thin section preparation, the Instituto Aragonés de Gestió n Ambiental (INAGA) for sampling licenses, and Dr Anne van der Weerd for field assistance. HA acknowledges the financial support of the Dutch Science Foundation (NWO-ALW). Dr Frits Hilgen is thanked for useful discussions and improvements on earlier versions of the manuscript. Prof. Ildefonso Armenteros, Dr Miguel Garcés and Dr Wan Yang are acknowledged for their constructive reviews.

REFERENCES

Abdul Aziz, H. (2001) *Astronomical Forcing in Continental Sediments*. PhD thesis, Utrecht University, Utrecht, the Netherlands.

Abdul Aziz, H., Hilgen, F.J., Krijgsman, W., Sanz, E. and Calvo, J.P. (2000) Astronomical forcing of sedimentary cycles in the middle to late Miocene continental Calatayud Basin (NE Spain). *Earth Planet. Sci. Lett.*, 177, 9–22.

Abdul Aziz, H., Krijgsman, W., Hilgen, F.J., Wilson, D.S. and Calvo, J.P. (2003a) An astronomical polarity timescale for the late Middle Miocene based on cyclic continental sequences. *J. Geophys. Res.*, 108, B3, 2159. doi:10.1029/2002JB001818.

Abdul Aziz, H., Sanz-Rubio, E., Calvo, J.P., Hilgen, F.J. and Krijgsman, W. (2003b) Palaeoenvironmental reconstruction of a middle Miocene alluvial fan to cyclic shallow lacustrine depositional system in the Calatayud Basin (NE Spain). *Sedimentology*, 50, 211–236.

Abdul Aziz, H., Van Dam, J., Hilgen, F.J. and Krijgsman, W. (2004) Astronomical forcing in Upper Miocene continental sequences: implications for the Geomagnetic Polarity Time Scale. *Earth Planet. Sci. Lett.*, 222, 243–258.

Albesa, J., Calvo, J.P., Alcalá, L. and Alonso Zarza, A.M. (1997) Interpretación paleoambiental del yacimiento de La Gloria 4 (Plioceno, Fosa de Teruel) a partir del análisis de facies y de asociaciones de gasterópodos y de mamíferos. *Cuad. Geol. Ibérica*, 22, 239–264.

Alonso Zarza, A.M. (2003) Palaeoenvironmental significance of palustrine carbonates and calcretes in the geological record. *Earth-Sci. Rev.*, 60, 261–298.

Alonso Zarza, A.M. and Calvo, J.P. (2000) Palustrine sedimentation in an episodically subsiding basin: the Miocene of the northern Teruel Graben (Spain). *Palaeogeogr. Palaeoclimatol. Palaeoecol.*, 160, 1–21.

Anadón, P. and Moissenet, E. (1996) Neogene basins in the eastern Iberian range. In: *Tertiary Basins of Spain* (Eds P.F. Friend and C.J. Dabrio), *World and Regional Geology Series*, 6, 68–71.

Anadón, P., Rosell, L. and Talbot, M.R. (1992) Carbonate replacement of lacustrine gypsum deposits in two Neogene continental basins, eastern Spain. *Sed. Geol.*, 78, 201–216.

Anadón, P., Ortí, F. and Rosell, L. (1997) Unidades evaporíticas de la zona de Libros-Cascante (Mioceno, Cuenca de Teruel): Características estratigráficas y sedimentológicas. *Cuad. Geol. Ibérica*, 22, 283–304.

Berger, A.L. (1978) Long-term variations of daily insolation and Quaternary climatic changes. *J. Atmos. Sci.*, 35, 2362–2367.

Broekman, J.A. (1983) Environments of deposition, sequences and history of Tertiary continental sedimentation in the Basin of Teruel-Ademuz (Spain). *Proc. K. Ned. Acad. Wet. Ser. B*, 86, 25–37.

Broekman, J.A., Besems, R.E., Daalen, P.v. and Steensma, K. (1983) Lithostratigraphy of Tertiary continental deposits in the Basin of Teruel-Ademuz (Spain). *Proc. K. Ned. Acad. Wet Ser. B*, 86, 1–16.

Buurman, P. (1980) Paleosols in the Reading Beds (Paleocene) of Alum Bay, Isle of Wight, U.K. *Sedimentology*, 27, 593–606.

Cohen, A.S. and Thouin, C. (1987) Nearshore carbonate deposits in Lake Tangayika. *Geology*, 15, 414–418.

Currey, D.R. (1990) Quarternary palaeolakes in the evolution of semidesert basins, with special emphasis on Lake Bonneville and the Great Basin, USA. *Palaeogeogr. Palaeoclimatol. Palaeoecol.*, 76, 189–214.

Dunham, R.J. (1962) Classification of carbonates according to their depositional texture. In: *Classification of Carbonate Rocks* (Ed. W.E. Ham), *AAPG Mem.*, 1, 108–121.

Dupont-Nivet, G., Krijgsman, W., Langereis, C.G., Abels, H.A., Dai, S. and Fang, X. (2007) Tibetan plateau aridification linked to global cooling at the Eocene-Oligocene transition. *Nature*, 445, 635–638.

Eardley, A.J., Shuey, R.T., Gvosdetsky, V., Nash, W.P., Picard, M.D., Grey, D.C. and Kukla, G.J. (1973) Lake cycles in the Bonneville Basin, Utah. *Geol. Soc. Am. Bull.*, 84, 211–216.

Folk, R.L. (1959) Practical petrographic classification of limestones. *AAPG Bull.*, 43, 1–38.

Foucault, A. and Mélières, F. (2000) Palaeoclimatic cyclicity in central Mediterranean Pliocene sediments: the mineralogical signal. *Palaeogeogr. Palaeoclimatol. Palaeoecol.*, 158, 311–323.

Freytet, P. and Verrecchia, E.P. (2002) Lacustrine and palustrine carbonate petrography: an overview. *J. Paleolimnol.*, 27, 221–237.

García, A. (1994) Charophyta: their use in paleolimnology. *J. Paleolimnol.*, 10, 43–52.

Gradstein, F.M., Ogg, J.G., Sith, A.G., Bleeker, W. and Lourens, L.J. (2004) A new Geologic Time Scale, with special reference to Precambrian and Neogene. *Episodes*, 27, 83–100.

Hazeleger, W., Molteni, F., Severijns, C., Haarsma, R., Bracco, A. and Kucharski, F. (2003) SPEEDO: a flexible coupled model for climate studies. *Exchanges*, 28, 1–3.

Hilgen, F.J., Abdul Aziz, H., Krijgsman, W., Langereis, C.G., Lourens, L.J., Meulenkamp, J.E., Raffi, I., Steenbrink, J., Turco, E., Van Vugt, N., Wijbrans, J.R. and Zachariasse, W.J. (1999) Present status of the astronomical (polarity) time-scale for the Mediterranean Late Neogene. *Phil. Trans. Roy. Soc. London A*, 357, 1931–1947.

Hüsing, S.K., Hilgen, F.J., Abdul Aziz, H. and Krijgsman, W. (2007) Completing the Neogene geological time scale between 8.5 and 12.5 Ma. *Earth Planet. Sci. Lett.*, 253, 340–358.

Kiefer, E. (1988) Facies development of a lacustrine tectosedimentary cycle in the Neogene Teruel-Ademuz Graben (NE Spain). *Neues Jb. Geol. Paläontol.*, 6, 327–360.

Laskar, J., Robutel, P., Joutel, F., Gastineau, M., Correia, A.C.M. and Levrard, B. (2004) A long term numerical solution for the insolation quantities of the Earth. *Astron. Astrophys.*, 428, 261–285.

Lindholm, R.C. and Finkelman, R.B. (1972) Calcite staining: semi-quantitative determination of ferrous iron. *J. Sed. Petrol.*, 42, 239–242.

Lourens, L.J. (2004) Revised tuning of Ocean Drilling Program Site 964 and KC01B (Mediterranean) and implications for the d18O, tephra, calcareous nannofossil, and geomagnetic reversal chronologies of the past 1.1 Myr. *Paleoceanography*, 19, PA3010. doi: 10.1029/2003PA000997.

Lourens, L.J., Hilgen, F.J., Shackleton, N.J., Laskar, J. and Wilson, D.S. (2004) The Neogene Period. In: *A Geologic Time Scale 2004* (Eds F.M. Gradstein, J.G. Ogg and A. Smith), pp. 405–440. Cambridge University Press, Cambridge.

Magri, D. and Tzedakis, P.C. (2000) Orbital signatures and long-term vegetation patterns in the Mediterranean. *Quartern. Int.*, 73/74, 69–78.

Molteni, F. (2003) Atmospheric simulations using a GCM with simplified physical parametrizations; Model climatology and variability in multi-decadal experiments. *Climate Dynam.*, 20, 175–191.

Normati, M. and Salomon, J. (1989) Reconstruction of a Berriasian lacustrine paleoenvironment in the Cameros basin (Spain). *Palaeogeogr. Palaeoclimatol. Palaeoecol.*, 70, 215–223.

Olsen, P.E. and Kent, D.V. (1996) Milankovitch climate forcing in the tropics of Pangaea during the Late Triassic. *Palaeogeogr. Palaeoclimatol. Palaeoecol.*, 122, 1–26.

Pérez, A., Luzón, A., Roc, A.C., Soria, A.R., Mayayo, M.J. and Sánchez, J.A. (2002) Sedimentary facies distribution and genesis of a recent carbonate-rich saline lake: Gallocanta Lake, Iberian Chain, NE Spain. *Sed. Geol.*, 148, 185–202.

Picard, M.D. and High, L.R. (1981) Physical stratigraphy of ancient lacustrine deposits. *SEPM Spec. Publ.*, 31, 233–259.

Platt, N.H. (1989) Continental sedimentation in an evolving rift basin: the lower Cretaceous of the western Cameros Basin (northern Spain). *Sed. Geol.*, 64, 91–109.

Platt, N.H. and Wright, V.P. (1991) Lacustrine carbonates: facies models, facies distributions and hydrocarbon aspects. *Spec. Publ. Int. Ass. Sediment.*, 13, 57–74.

Rosen, M.R. (1994) The importance of groundwater in playas: a review of playa classifications and the sedimentology and hydrology of playas. In: *Paleoclimate and Basin Evolution of Playa Systems* (Ed. M.R. Rosen), *GSA Volume Special Paper*, 289, 1–18.

Rossignol-Strick, M. (1983) African monsoons, an immediate climate response to orbital insolation. *Nature*, 304, 46–49.

Sagri, M., Abbate, E. and Bruni, P. (1989) Deposits of ephemeral and perennial lakes in the Tertiary Daban basin (Northern Somalia). *Palaeogeogr. Palaeoclimatol. Palaeoecol.*, 70, 225–233.

Sanz, M.E., Alonso-Zarza, A.M. and Calvo, J.P. (1995) Carbonate pond deposits related to semi-arid alluvial systems: examples from the Tertiary Madrid basin, Spain. *Sedimentology*, 42, 437–452.

Sierro, F.J., Flores, J.A., Zamarreño, I., Vázquez, A., Utrilla, R., Francés, G., Hilgen, F.J. and Krijgsman, W. (1999) Messinian pre-evaporite sapropels and precession-induced oscillations in western Mediterranean climate. *Mar. Geol.*, 153, 137–146.

Sierro, F.J., Ledesma, S., Flores, J.-A., Torrescusa, S. and Martínez del Olmo, W. (2000) Sonic and gamma-ray astrochronology: cycle to cycle calibration of Atlantic climatic records to Mediterranean sapropels and astronomical oscillations. *Geology*, 28, 695–698.

Steenbrink, J., Van Vugt, N., Hilgen, F.J., Wijbrands, J.R. and Meulenkamp, J.E. (1999) Sedimentary cycles and volcanic ash beds in the Lower Pliocene lacustrine succession of Ptolemais (NW Greece): discrepancy between $^{40}Ar/^{39}Ar$ and astronomical ages. *Palaeogeogr. Palaeoclimatol. Palaeoecol.*, 152, 283–303.

Tuenter, E., Weber, S.L., Hilgen, F.J. and Lourens, L.J. (2003) The response of the African summer monsoon to remote and local forcing due to precession and obliquity. *Global Planet. Change*, 36, 219–235.

Türkmen, I. and Kerey, I.E. (2000) Alluvial and lacustrine facies of the Yeniçubuk formation (lower-middle Miocene), Upper Kizilirmak basin, Tü rkiye (Turkey). In: *Lake Basins through Space and Time* (Eds E.H. Gierlowski-Kordesch and K. Kelts), *AAPG Stud. Geol.*, 46, 449–464.

Van Dam, J., Abdul Aziz, H., Alvarez Sierra, M.A., Hilgen, F.J., Van den Hoek Ostende, L.W., Lourens, L.J., Mein, P., Van der Meulen, A.J. and Pelaez-Campomanes, P. (2006) Long-period astronomical forcing of mammal turnover. *Nature*, 443, 687–691.

Vázquez, A., Utrilla, R., Zamarreño, I., Sierro, F.J., Flores, J.A., Francés, G. and Bá rcena, M.A. (2000) Precession-related sapropelites of the Messinian Sorbas Basin (South Spain): paleoenvironmental significance. *Palaeogeogr. Palaeoclimatol. Palaeoecol.*, 158, 353–370.

Warren, J. (1999) *Evaporites: Their Evolution and Economics*. Blackwell Science, Oxford, 438 pp.

Weedon, G.P. (2003) *Time-series Analysis and Cyclostratigraphy – Examining Stratigraphic Records of Environmental Cycles*. Cambridge University Press, Cambridge, 259 pp.

Wright, P.V. and Marriott, S.B. (2007) The dangers of taking mud for granted: Lessons from Lower Old Red Sandstone dryland river systems of South Wales. *Sed. Geol.*, 195, 91–100.